Electronic Supplementary Material (ESI) for Nanoscale.
This journal is © The Royal Society of Chemistry 2020

Supporting Information

Title: Broadband Chiral Hybrid Plasmon Modes on Nanofingernail Substrates

Paulina Librizzi[+], *Aneek Biswas*[†,∆], *Roger Chang*[+], *Xiang-Tian Kong*[#], *Matthew Moocarme*[†,∆], *Gaurav Ahuja*[#], *Ilona Kretzschmar*[+,*], *and Luat T. Vuong*,[†,∆,#,*]

[+] Department of Chemical Engineering, City College of New York of the City University of New York (CUNY), New York, New York 10031, United States,

[†] Department of Physics, Graduate Center of the City University of New York (CUNY), New York, New York 10016, United States

[∆] Department of Physics, Queens College of the City University of New York (CUNY), Queens, New York 11367, United States

[#] Department of Mechanical Engineering, Bourns Hall, University of California at Riverside, Riverside, California 92521, United States

Characterization of Thickness

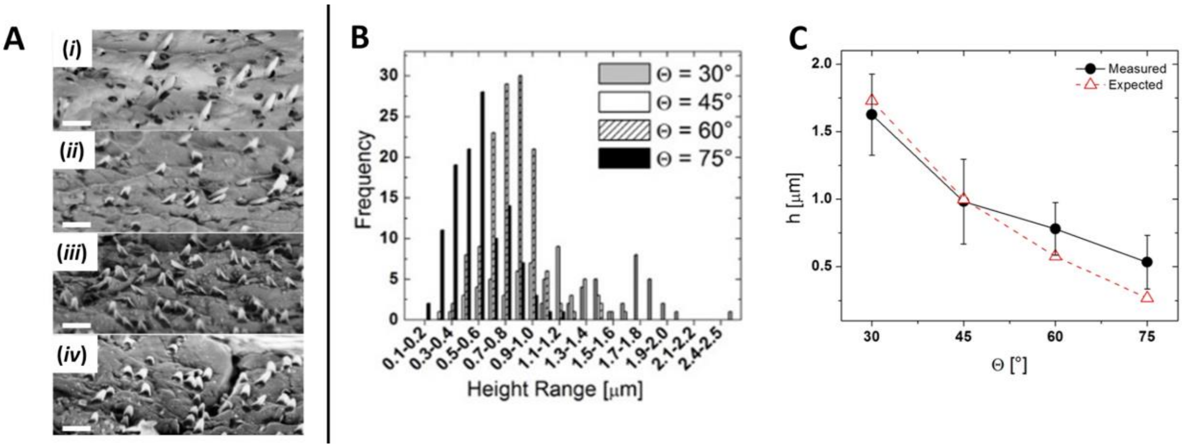

Figure S1. (A) SEM images of nanofingernails fabricated at θ = (i) 30° (ii) 45° (iii) 60° and (iv) 75° (scale bar: 5μm). (B) Frequency distribution of nanofingernail heights at each angle. Nanofingernails uniformity depends on the regularity of the template. The extrinsically-chiral orientation of the nanofingernail is aligned via I-GLAD. (C) Nanofingernail height distributions. Comparison of expected and measured nanofingernail heights at each deposition angle.

Composite Au-Ag hybrid nanofingernails are fabricated at four different deposition angles, θ = 30°, 45°, 60° and 75°, using a TEPC template with 1 μm wide pores. The structures are characterized using scanning electron microscopy (SEM) on an angled sample holder [**Fig. S1A**]. The number of successfully fabricated nanofingernails is counted with ImageJ and a frequency distribution for their height is generated for each of the four deposition angles [**Fig. S1B**]. Irregularities are largely attributed to the TEPC template as mentioned previously, however dimensional variations associated with the I-GLAD process also increase for smaller deposition angles θ; any variation in the pore angle φ is associated with large changes in height [**Fig. 1C**]. The dimensional deviation at large θ is due to the surface roughness of the TEPC template, which favors nanofingernail formation in pores that are located in sections of the template that face towards the source. Large and nearly identical numbers of nanofingernails are observed at θ = 60° and θ = 75°. At θ = 30°, the fewest number of nanofingernails are observed, the count being 75% fewer than the highest total, whereas at θ = 45°, about 60% fewer structures are observed. Overall, the smallest h is 0.1 μm and is achieved at θ = 75°, while the largest h is 2.6 μm and is achieved at θ = 30°. **Figure S1C** illustrates the relationship between the deposition angle and the average measured fingernail height in comparison with the height calculated in equation 1, with w set to 1μm and (φ) set to 0°. The thickness of the nanofingernails depends on the amount of metal deposited and is monitored during the deposition procedure. The density of the nanoparticles depends on the lift-off process.

The nanofingernail thickness can also be tuned. The thickness of the nanofingernails depends on the amount of metal deposited and the deposition angle, θ. However, determination of the actual fingernail thickness is complicated by the fact that the nanofingernail fabrication occurs on curved surfaces that are angled with respect to the metal vapor source. Rather than relying solely on the known deposition thickness, the average thickness of a nanofingernail is instead estimated by dividing the volume of deposited metal by the nanofingernail surface area.

The nanofingernail volume, V, is calculated based on two parameters: (1) the known deposition thickness d as measured by the crystal balance thickness monitor and (2) the effective pore area, A_{eff}, that is accessible to the metal vapor as it descends from the source. A_{eff} is the projection of the pore opening onto a plane parallel to the source. When θ = 0°, A_{eff} is equal to the full circular pore opening. However, as θ increases, A_{eff} becomes oval and decreases in size until it is equal to 0 at θ = 90°. The volume of a nanofingernail can therefore be expressed as the product of the known deposition thickness d ($d = 125$ nm in the case presented here) and the effective pore area A_{eff} at each θ:

$$V = d\,\pi\,(\cos\theta)\,(w/2)^2 \tag{2}$$

To obtain the surface area S_L of a nanofingernail, one can approximate the nanofingernail shape as a cylindrical hoof created by the intersection of a hollow cylinder and a plane. The lateral surface area of such a shape is given as:[5]

$$S_L = 2hR\left(\frac{sinsin\,\alpha - \alpha coscos\,\square}{1 - coscos\,\square}\right) \tag{3}$$

where h is the nanofingernail height, R is the pore radius and $\alpha = \pi/2$ radians (because the footprint of the nanofingernail is a half-circle). When the volume V is divided by the lateral surface area S_L, an estimate of the average nanofingernail thickness is obtained. **Table S2** summarizes the calculated A_{eff}, V, and S_L at the various θ. As can be seen from **Table S2**, despite the smaller volume of metal deposited at higher deposition angles, the lateral surface area S_L decreases even faster with increasing θ such that the nanofingernail thickness is estimated to be nearly twice as thick at θ = 75° compared to θ = 30°.

Table S2. Estimation of Nanofingernail Thickness (z). For each deposition angle θ and effective pore area A_{eff}, the nanofingernail volume (V) and the lateral surface area (S_L) are calculated according to Equations (2) and (3). Dividing V by S_L gives the nanofingernail thickness (z).

Θ [°]	A_{eff} [10^5 nm^2]	V [10^7 nm^3]	*H* [nm]	S_L [10^6 nm^2]	z = V/S_L [nm]
30±2	6.8 ± 0.1	8.5 ± 0.2	1,730	1.73	49 ± 1
45±2	5.6 ± 0.2	6.9 ± 0.3	1,000	1.00	69 ± 3
60±2	3.9 ± 0.2	4.9 ± 0.3	580	0.58	85 ± 5
75±2	2.0 ± 0.3	2.5 ± 0.3	270	0.27	94 ± 12

The high degree of tunability and other advantages in terms of cost and flexibility, demonstrate that the fabrication method presented here is a promising avenue to achieve arrays of optically active hybrid metal nanostructures.

Characterization of fingernail density

The porosity of a track etched polycarbonate membrane with 1000 nm pores is 15.7%. This means that per square millimeter of template, the area encompassed by pores is roughly 157,000 um2. With each pore having an area of ~0.785 um^2, each millimeter has around 200,000 pores. Experimentally, more fingernails are left upright at high deposition angles than at low deposition angles. This is due to a decrease in the thickness of the deposited nanofingernail. The thinner nanofingernails that result from lower deposition angles do not survive the cleaning process, in which polycarbonate template is removed via chloroform. To remove the template, the side of the sample which faced the source was placed down onto a silicon wafer or glass slide (depending on the characterization method), and chloroform was pipetted dropwise onto the hydrophobic surface. As the chloroform rinsed away the polycarbonate, the thinner structures are washed away.

Circular dichroism (CD) measurements

Circular dichroism (CD) spectroscopy, which measures the difference in the absorption of left (σ_-) and right-handed (σ_+) circular polarizations as a function of wavelength, is employed to show the optical activity and the impact of the bimetallic nature of the nanofingernails [**Fig. S3**]. At normal incidence, the substrate on which the nanofingernails sit lies in the *x-y* plane, and circularly-polarized light is incident along the -z-direction [**Fig. S3A**]. The characterization of $CD = 2(T_+ - T_-)/(T_+ + T_-)$ is the normalized difference in orthogonal circular-polarization transmission $T_{\pm}$., i.e., the difference in right- and left-handed circular polarized light interaction with the nanostructure. The values of the CD in percent are converted to ellipticity in degrees with the relation, $\varphi = 2.303*180/4\pi*\{\log[(2+CD)/(2-CD)]\}$. The data in **Figs. S3(B-D)** are representative measurements of samples prepared at θ = 45°, 60°, and 75°, respectively, rotated clock- (−γ) and counterclock-wise (+γ) around y-axis in x-z plane, where deviations of 0.05% CD would be attributed to temporal variations in the light source alone. The CD measurements of the tilted nanofingernails are normalized to the measurements of the normally-incident nanofingernails (γ = 0°). In general, CD is negligible when the direction of light is aligned with the long axis of the nanofingernails (here, the *z*-axis). However, when the nanofingernail orientation varies with respect to either the illuminating direction of light (rotation around y-axis) or the substrate **(**rotation around *x*-axis not shown), the CD arises in a manner that is unique and specific to the nanofingernail and illumination geometry.

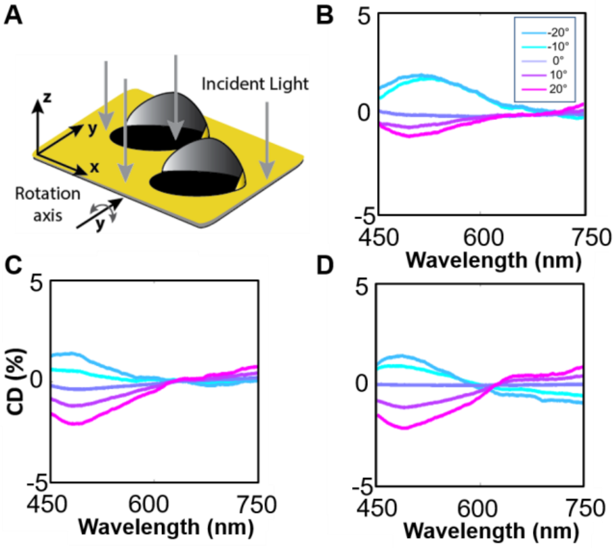

Figure S3. (A) Schematic showing the geometry of the CD measurement of a planar, low-density (2% fill factor), random array of aligned nanofingernails (θ = 75°) when rotated clock (−γ) and counterclock-wise (+γ) around the y-axis in the *x-z* plane. CD results from nanofingernails when silver (75 nm)/gold (50 nm) deposition is performed at (B) θ = 45° (C) θ = 60° and (D) θ = 75°.

A CD response of 2% is achieved by rotating the nanofingernails around the *y*-axis [**Fig. S3**]. In this nanofingernail orientation, the nanofingernail arc represents half of a helix that spirals around the direction of light propagation, or the *z*-axis. The measured CD is reduced when the nanofingernail alignment is not aligned normal to the sample surface. When the nanofingernails are rotated around the *y*-axis in the *x*-*z* plane, the CD is symmetric across positive (+γ) and negative (−γ) illumination angles as expected from the symmetry of the nanofingernails. While **Figures S3(B-D)** should show strong symmetry around normal incidence, slight deviations from symmetry around $\gamma = 0°$ are observed due to the rotation of the nanofingernails around the z-axis of approximately 10°.

Magnetic Fields Surrounding Nanofingernail Structure

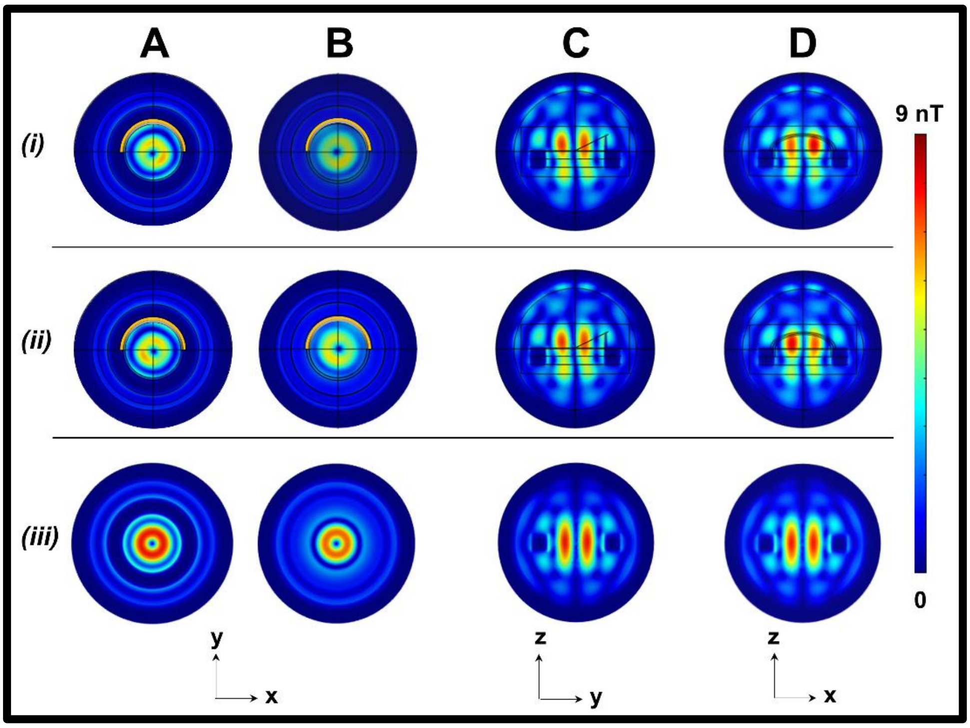

Figure S4. Time-averaged magnitudes of the scattered or longitudinal magnetic fields (z-component) λ = 580nm in the *x-y* plane (A) in the center of the metal film (B) at the bottom plane of the metal film (C) in the *y-z* plane (D) in the *x-z* plane for (i) left-handed (ii) right-handed circularly-polarized light on a nanofingernailed aperture (iii) on an aperture alone.

Analysis of Angular Momentum Dynamics in Nanofingernail Scattering

It is valuable to comment precisely on the light angular momenta imparted by the nanofingernail geometry, since the nanostructure absorption and scattering events (or other nonparaxial phenomena) blur the strict definitions of optical spin and orbital angular momentum. In addition, our fundamental understanding of the chiral power flow is relevant to applications of chiral molecular detection.

Firstly, even though the scattered field from a round aperture carries a vortex phase profile that changes direction with incident circular handedness, the scattered light does not carry orbital angular momentum. Light will, however, carry intrinsic orbital angular momentum when immediately absorbed by an intrinsically-chiral structure, or extrinsic orbital angular momentum when immediately absorbed from an extrinsically-chiral nanostructure. Subsequent to this event, the interpretation of light momenta depends on the direction that light is propagating. In the presence of loss with the excitation of plasmons here, the near fields or waves do not propagate to the far-field, and it is not clear how angular momentum flux is conserved. We anticipate that the 3-D chiral scattered-field hotspots that spiral as a function of propagation may lead to a presence of spin-to-orbital angular momentum conversion and mild nonreciprocal effects. This can be viewed in the magnetic fields that are parallel to the surface.

Chiral changes in power flow result from the presence of the nanofingernail in the *x-z* and *y-z* planes. Unlike the power flow in the *x-y* planes, which is spiral because of the illuminating circular polarization, the power flow that represents a handedness to the angular momentum flux in the *x-z* and *y-z* planes do not exhibit radial symmetry. **Figure S5** shows that the presence of the nanofingernails also leads to additional vorticial flows that are not observed with the aperture alone. Even though the electromagnetic field intensities far from the nanostructure are small, these power-flow dynamics may influence the movement of charged particles in microfluidic experiments.

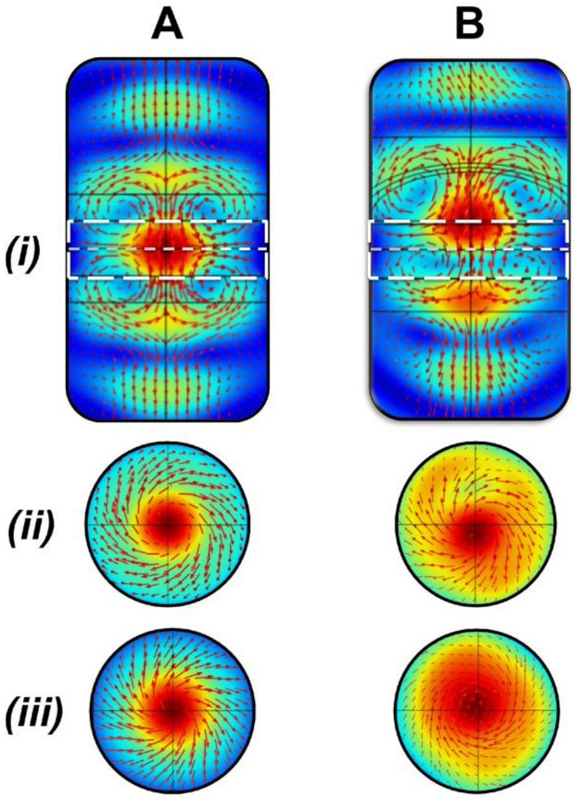

Figure S5. Time-averaged electric-field amplitudes (colorplot) and power flow vector or Poynting (arrows) for λ = 640nm light for (A) aperture alone (B) right-handed circularly-polarized light on the nanofingernail (i) in the *x-z* plane and in the *x-y* plane (ii) at the top plane of the substrate (iii) at the bottom plane of the substrate.

Analysis of Multipolar Modes Supported by Nanofingernails

We study the plasmonic modes supported by the nanofingernails under visible illumination. The diameter of the holes under the nanofingernails is $w = 1.5$ μm. Although these out-of-plane structures are on the nanoscale, the holes are about twice the spectral interval of interest in this paper. Consequently, all the modes in the nanofingernails are multipolar modes, which are highly localized and very sensitive to the geometrical parameters. Our geometry models are based on the fabrication process of the physical vapor deposition. The thicknesses of the gold and silver layers are 75 nm and 50 nm, respectively. Here we assume the nanofingernails are perpendicular to the substrate (**Figure S6**). To gain an understanding of the effects of each component of the structure, we first separately study the optical response of the tilted holes and compare the spectra with that of the nanofingernails on the tilt holes.

Figure S7 shows the absorption and transmission spectra of the square array of nanofingernails with 60-degree deposition angle (Figure S4) illuminated by linearly polarized beams. The spectra are calculated with the finite element software of COMSOL. The optical constants of gold and silver are taken from the tabulated data from Johnson and Christy. The substrate is assumed to be dispersionless with refractive index of 1.5. We observe the following points from the spectra: (1) multiple peaks are present in the visible spectral interval (400 nm < λ_0 < 800 nm) for both the structures and (2) with only a few exceptions, for most visible wavelengths, the holes have greater transmission and less absorption than the nanofingernails. The first point explains the broadband transmission feature of the experimentally measured spectra – the bunch of individual peaks could merge with each other and form a broad band due to homogeneous and inhomogeneous broadenings (which are caused by statistical geometrical parameters in the sample and statistical factors in the measurement). The second point indicate that ohmic loss is a major damping pathway for the plasmonic multipolar modes.

The multipolar nature of the plasmonic modes is demonstrated by the surface charge distributions shown in **Figure S8**. These maps are given at the major absorption peaks in **Figure S8 (a,b)**. The standing wave pattern of the charge oscillation is not symmetric along the *x*-direction. However, because of the geometry symmetry along *y*-direction, we could always observe a charge neutral plane (white area along *x*-axis) for *y*-polarized incident light. **Figure S9** shows the major transmission pathways of the incident light at the peaks of the transmittance spectra. In view of the complexity of the geometry, these standing waves of surface charges shown in **Figure S8** and transmission pass ways in **Figure S9** would highly sensitive to the geometrical and material parameters.

Figure S10 shows the absorption and transmission peaks shift dramatically when changing the height of the structure. Nevertheless, we consistently observe multiple peaks in the visible spectral interval of wavelengths 400 – 800 nm. **Figure S11** shows the magnitude and position of the absorption and transmission maxima depend on the material properties, indicating the optical response is tuned by adjusting the thickness and materials of the layers. Moreover, silver structures present lower loss and greater transmission.

1. P. B. Johnson, R. W. Christy, Optical constants of the noble metals. Phys. Rev. B 6, 4370–4379 (1972).

(a) Nanofingernails on tilt holes

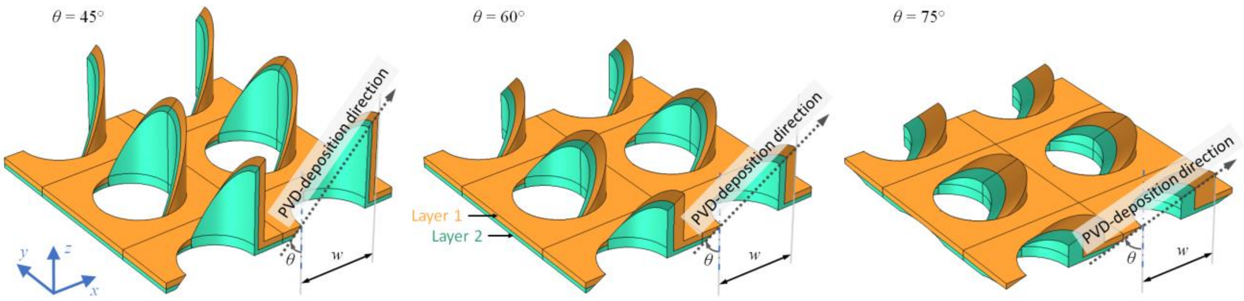

(b) Tilt holes

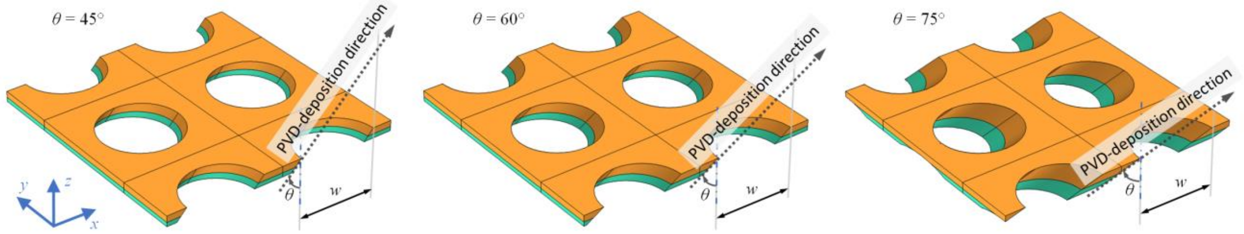

Figure S6. Geometry models of the nanofingernails and their corresponding tilted nanoholes. The hole diameter is fixed at $w = 1$ μm. We assume the metal atoms are deposited on a perfect template such that all nanofingernails are perpendicular to the substrate and form a square array. For the array we assume a fixed period of 1.5 μm. Then the height of the nanofingernail is only determined by the hole diameter w and the deposition angle θ.

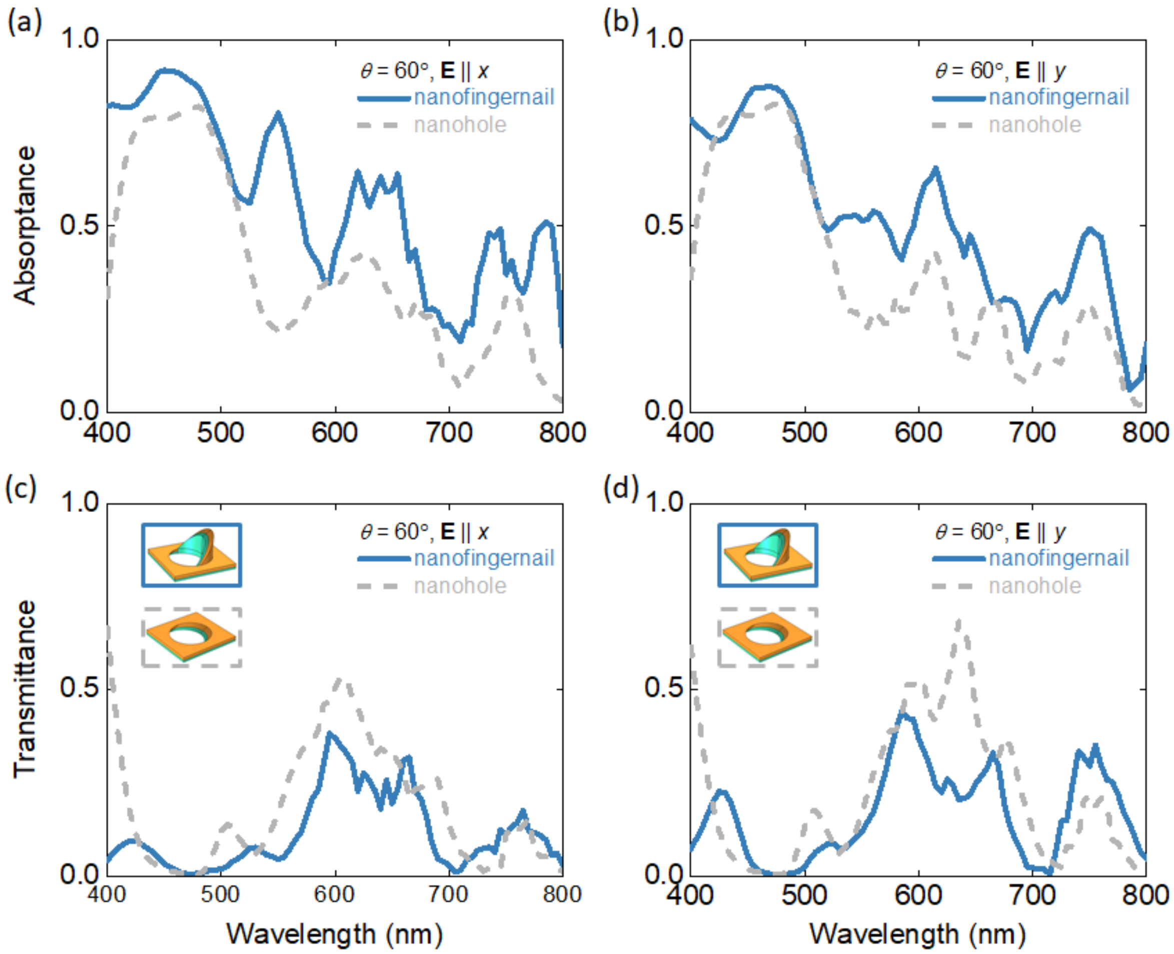

Figure S7. Absorbance (a, b) and transmittance (c, d) of the square arrays of nanofingernails and tilt holes with 60-degree deposition angle and 1 µm hole diameter. The arrays are illuminated by linearly polarized light. (a, c) show the spectra with *x*-polarized beam; (b, d) show the spectra with *y*-polarized beam. The coordinate system is defined in **Figure S6**.

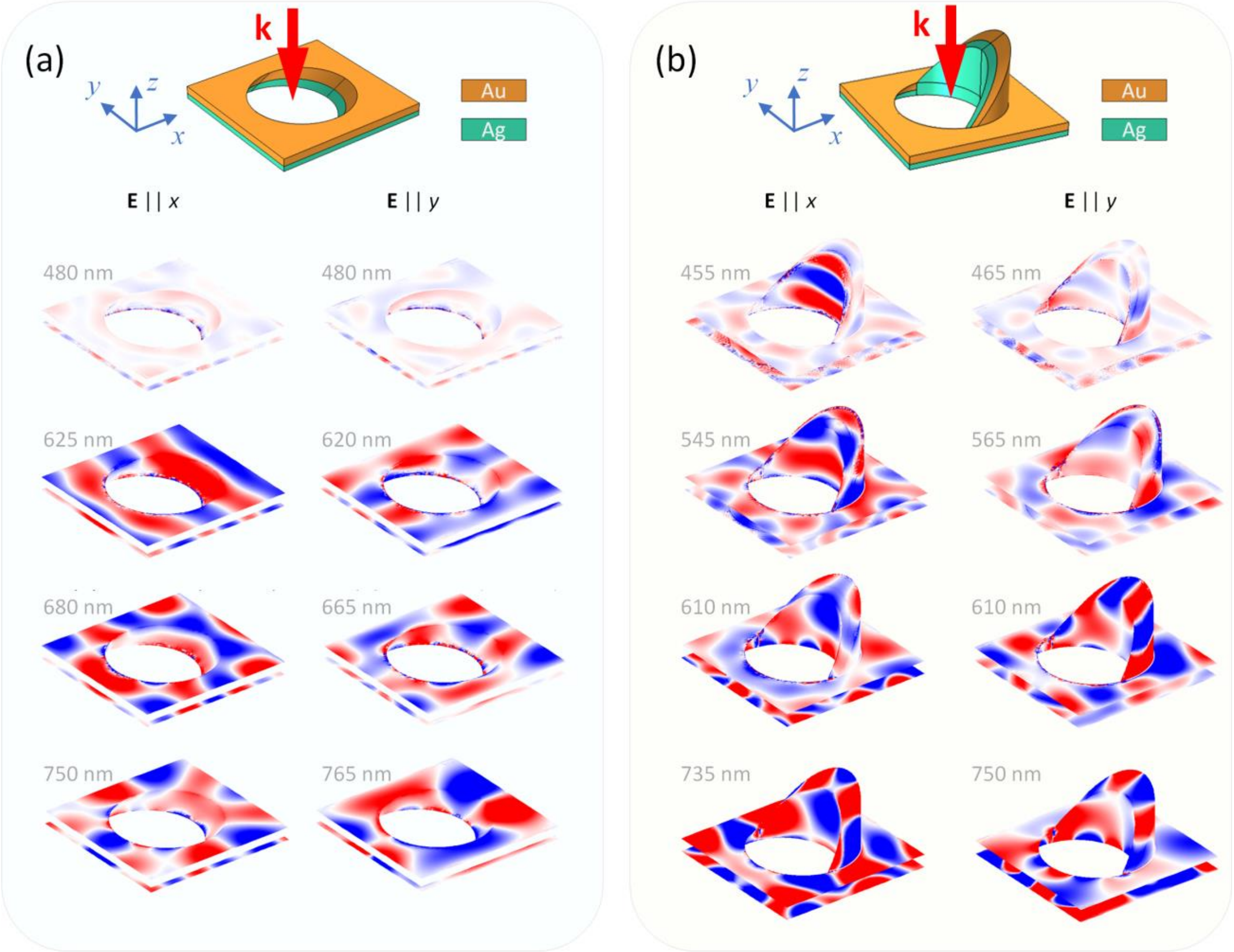

Figure S8. Surface charge distribution of the nanohole (a) and nanofingernail (b) at various absorption peaks with linear-polarized light. The reddish and bluish colors show positive and negative charges respectively. The deposition angle of the structures (see **Figure S6**) is 60 degrees.

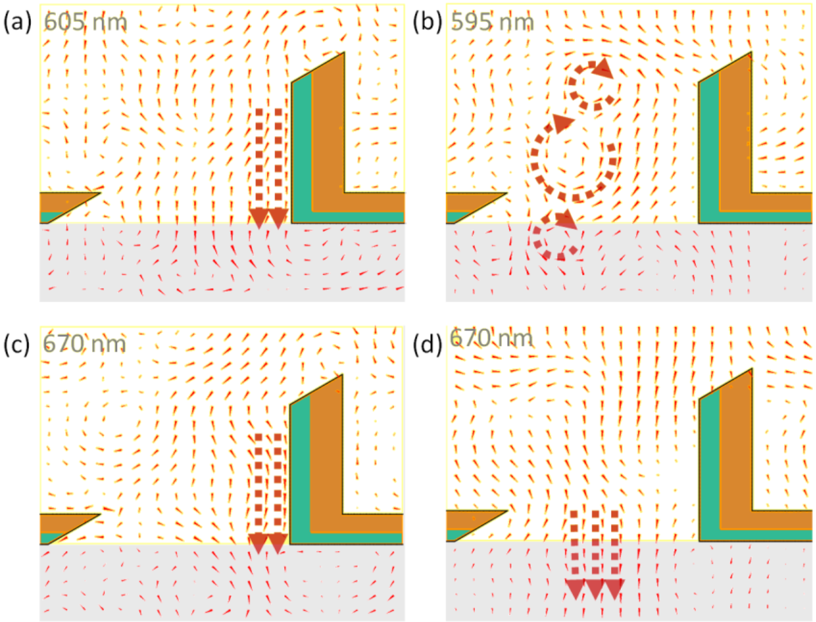

Figure S9. Power flux at transmission peaks with linearly polarized light. (a, c) incident beam is *x*-polarized; (b, d) incident beam is *y*-polarized. At the transmission peaks, the out-of-plane part of the geometry could either guide the incident wave to the exit of the hole or trap the incident light near the hole and only weakly backscatter the incident power (b, d). When the former happens the power flux is parallel to the metal walls (a, c).

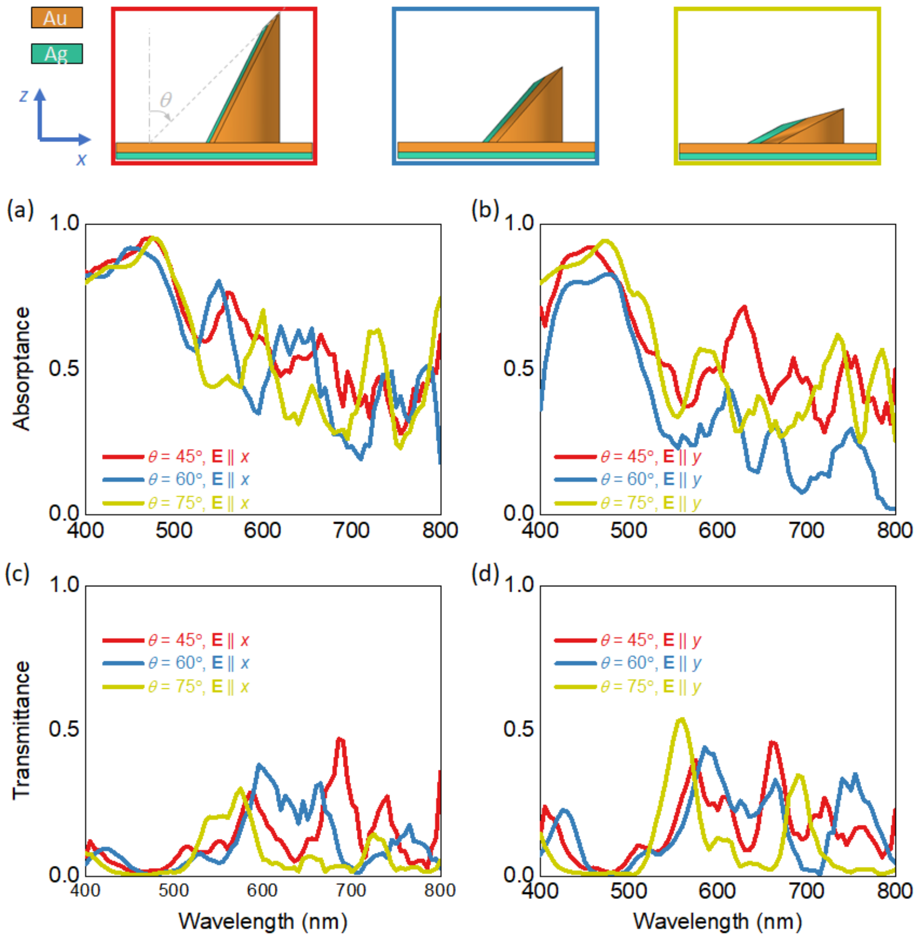

Figure S10. (a,b) Absorbance and (c,d) transmittance of nanofingernails with deposition angle θ = 45, 60, 75 degrees. The spectral peaks are highly sensitive to the height of the structure.

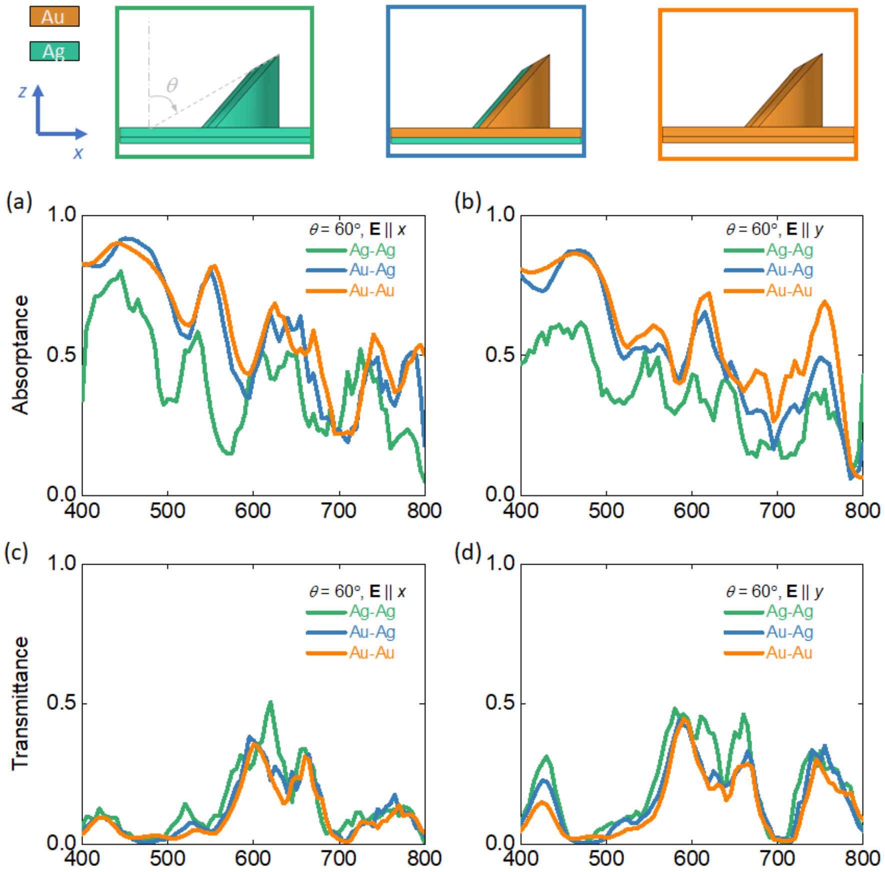

Figure S11. (a,b) Absorption and (c,d) transmission of nanofingernails with different compositions.